LA-UR-04-5088

Approved for public release; distribution is unlimited.

Title: A Numerical Performance Model for Piezoelectrical Actuators for Jet Noise Reduction

Author(s): Bryan (Bucky) A. Kashiwa,Los Alamos National Laboratory
G.W. Butler, The Boeing Company

Submitted to: Published in Proceedings:
"ACTIVE 04" The 2004 International Symposium on Active Control of Sound and Vibration
Williamsburg, Virginia
September 20-22, 2004

A Numerical Performance Model for Piezoelectric Actuators for Jet Noise Reduction

Bryan (Bucky) A. Kashiwa, *T-3 Fluid Dynamics Group, LANL-Los Alamos*
G.W. Butler, Aeroacoustics and Fluid Mechanics-The Boeing Company -Seattle, WA
"ACTIVE 04"
The 2004 International Symposium on Active Control of Sound and Vibration
Williamsburg, Virginia
September 20-22, 2004

ABSTRACT

The use of small-scale disturbances to control turbulence production and sound generation in regions of high shear has long been a topic of interest. We have previously reported the use of piezoelectrically driven, tab-type actuators to drive disturbances in the initial shear layer of a cold jet to accomplish this task. Particle imaging velocimetry along with phased array and far field microphones were used to interrogate the flow and acoustic fields, respectively. The complexities of turbulent flows, along with the strong interaction between the actuators and the fluid, make optimization of the actuator system difficult. We are therefore developing a numerical actuator performance model to gain insight into the actuator-flow physics. Los Alamos National Laboratory's (LANL) CFDLib provides the framework of our fluid-structure model. CFDLib is a library of stable and mature algorithms that can be assembled to address a wide-variety of problems. We utilize the generalized 3-D URANS multifluid algorithms with a two-fluid model that allows us to describe the motion of both gas and actuators on the same computational grid. The paper describes the modeling approach and presents initial comparisons with recent particle imaging velocimetry measurements.

This work was carried out under auspices of the National Nuclear Administration of the U.S. Department of Energy at Los Alamos National Laboratory under Contract No. W-7405-ENG-36.

Williamsburg, Virginia

ACTIVE 04

2004 September 20-22

A Numerical Performance Model for Piezoelectric Actuators for Jet Noise Reduction

G.W. Butler
Aeroacoustics and Fluid Mechanics
The Boeing Company
Seattle, WA
bill.butler@boeing.com

B. A. Kashiwa
Theoretical Division
Los Alamos National Laboratory
Los Alamos, NM
bak@lanl.gov

ABSTRACT

The use of small-scale disturbances to control turbulence production and sound generation in regions of high shear has long been a topic of interest. We have previously reported the use of piezoelectrically driven, tab-type actuators to drive disturbances in the initial shear layer of a cold jet to accomplish this task. Particle imaging velocimetry along with phased array and far field microphones were used to interrogate the flow and acoustic fields, respectively. The complexities of turbulent flows, along with the strong interaction between the actuators and the fluid, make optimization of the actuator system difficult. We are therefore developing a numerical actuator performance model to gain insight into the actuator-flow physics. Los Alamos National Laboratory's (LANL) CFDLib provides the framework of our fluid-structure model. CFDLib is a library of stable and mature algorithms that can be assembled to address a wide-variety of problems. We utilize the generalized 3-D URANS multifluid algorithms with a two-fluid model that allows us to describe the motion of both gas and actuators on the same computational grid. The paper describes the modeling approach and presents initial comparisons with recent particle imaging velocimetry measurements.

1. INTRODUCTION

The use of small-scale disturbances to control turbulence production and sound generation in regions of high shear has long been a topic of interest. Many early studies employed acoustic excitation to alter the initial growth rates of mixing layers.[1-6] From a noise reduction perspective, the production of turbulent kinetic energy (κ) and far field noise are intimately connected. The goal is to carefully tailor the actuator geometries and operating characteristics to reduce the production of turbulence energy at large-scales and their subsequent contribution to the low frequency jet noise spectrum. This typically requires stringent control of excitation frequencies and amplitudes to avoid large scale mixing and subsequent noise production. Piezoelectric actuators have recently been considered for this task. They have been used to excite the initial shear layer of jets to reduce their far field noise signature.[7-11] Although significant changes in the near-field turbulence spectrum have been demonstrated, relatively small decreases in far-field sound levels have been measured. It is clear that the relationship between flow field perturbations and the far-field sound spectrum is not yet understood.

We have previously reported on the use of piezoelectrically driven, tab-type actuators to generate disturbances in the initial shear layer of a cold jet.[12] Particle imaging velocimetry (PIV) along with phased array source imaging and far field microphones were used to interrogate the flow and acoustic fields. The installed actuators are shown in the photograph of Figure 1. The conical nozzle converges at 4.5° to a 6.985 cm exit diameter (D). The actuators are fabricated from 0.0394 cm spring steel stock and mounted the nozzle exit plane. They have an active (immersed) length of 1.32 cm, width of 1.05 cm, and are inclined at 24° with respect to the flow centerline. The piezo-electric driver material is bonded to the external surface (see insert of Figure 1). For the work reported here, 13 actuators were driven in phase at 1450 Hz with an estimated tip-to-tip displacement of 0.2 mm.

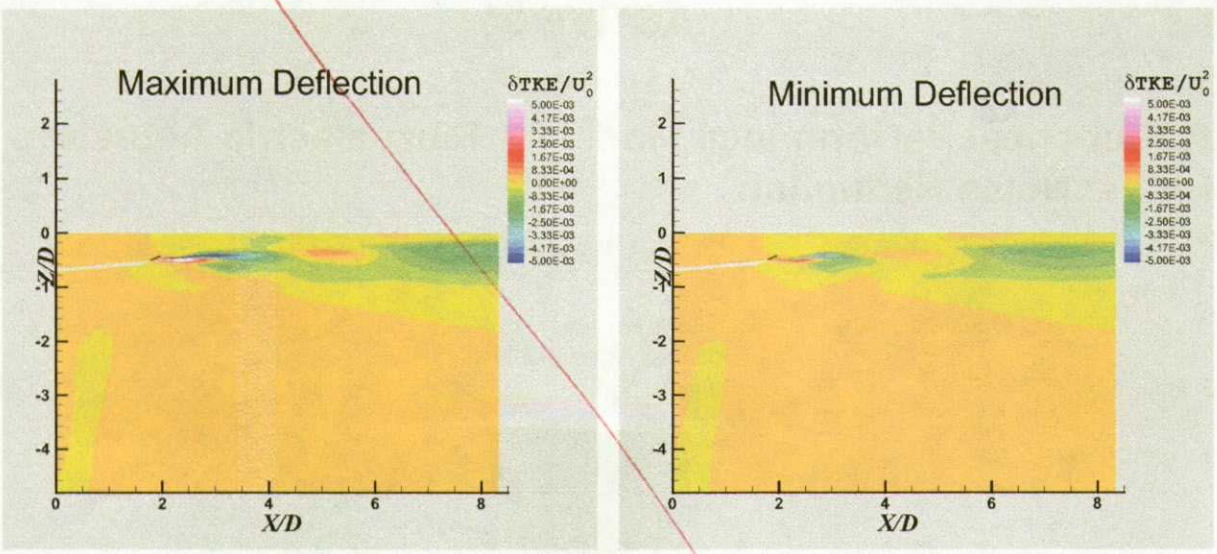

Figure 15. Instantaneous changes in turbulent kinetic energy distribution at maximum and minimum actuator deflection. Referenced to the stationary actuator flow field with $U_o = 3.122 \times 10^4$ cm/sec.

The actuators produced a small energy reduction at large turbulence length scales and a commensurate energy increase at smaller (dissipation) scales. Benefits gained in the low frequency portion of the noise spectrum thus occurred at the expense of increases in the high frequency spectrum. With active control, the peak overall sound pressure level (OASPL) shifted to lower emission angles and decreased in magnitude by approximately 1dB.

The complexities of turbulent flows, along with the strong interaction between the actuators and the fluid, make optimization of the actuator system difficult. For this reason, we have pursued the development of a numerical performance model to complement our experimental effort. It provides a tool to both evaluate new actuator concepts and to shape experimental strategy. In this paper we present an overview of the model and demonstrate the feasibility of this approach using initial comparisons with PIV data.

2. MODELING APPROACH

Los Alamos National Laboratory's (LANL) CFDLib provides the framework for our modeling effort.[13,14] CFDLib is a library of algorithms that can be assembled to address a wide-variety of problems. The time-dependent, Reynolds-Averaged Navier-Stokes equations are solved for this study. For the turbulence stress, a high Reynolds number κ - ε model with a one-seventh power law wall stress is used. In the absence of any mechanical excitation, this is a standard model. Mechanical excitation near the jet exit is accomplished by inserting a time-dependent force, whose magnitude is gauged on the expected force that a submerged, moving actuator, would exert on the flow.

The force due to a moving actuator changes in both time and space, because its orientation and velocity relative to the exhaust flow changes. This force is represented in the flow by means of a two-field model, and corresponding solution scheme. The two-field method used here is actually a subset of a multifield method used for dynamical fluid-structure interaction studies, in which the submerged structure is, in general, permitted to exhibit a dynamical response to the fluid loading and vice versa[15].

Let field number one be the exhaust gas, and let field two be the moving actuator. Accordingly, $[\rho_1, \vec{u}_1, p, \widetilde{R}_1, \theta_1]$ are the total mass density, velocity, pressure, Reynolds stress, and volume fraction for the gas. Let $\vec{u}_2$ be the velocity at any point in the moving actuator. The equation of motion for the gas is

$$\rho_1 \dot{\vec{u}}_1 = -\theta_1 \nabla p - \nabla \cdot \rho_1 \widetilde{R}_1 + \theta_1 \theta_2 \widetilde{K} \cdot (\vec{u}_2 - \vec{u}_1)$$

where the force is modeled with a tensor-valued coefficient ($\widetilde{K}$, having only positive elements) projected onto the relative velocity vector. The deviatoric stress due to the fluid viscosity is neglected here, and a perfect gas equation of state furnishes the pressure. Kashiwa et al describe the numerical method for solution of this and the remaining conservation equations in Reference 14. Briefly, this numerical method is a semi-implicit scheme designed to be free of any stability condition on the time step due to the speed of pressure waves or the magnitude of the interaction force. Acceleration due to the Reynolds stress and changes due to advection are computed with an explicit time-integration; hence the method respects an explicit stability condition based on the turbulent diffusion speed, and on the fluid speed.

The presence of the moving actuator, within the fluid computational domain, is created by a collection of mass markers. Each marker is assigned a fraction of the total actuator volume, and has a time-dependent (programmed) velocity corresponding to the rigid-body motion of the actuator; each marker also has a unit normal that is associated with the instantaneous actuator orientation. The position, velocity, volume, and local normal constitute the state of each marker, the aggregate of which is the state of the actuator. To begin each time increment, the marker state is interpolated from marker coordinates to grid coordinates; hence, for example, $\vec{u}_2(\vec{x}, t)$ becomes the value of the actuator velocity at a given location, and time t. In this way, the two-field method used here emulates the Immersed Boundary Method introduced by Peskin[16].

Let the local unit normal to the actuator be $\hat{n}(x,t)$, which in the present case is simply a function of time. The component of force normal to the actuator is modeled by $C_\perp \hat{n}\hat{n} \cdot (\vec{u}_2 - \vec{u}_1)$ and the component parallel to the actuator is $C_\parallel (\widetilde{I} - \hat{n}\hat{n}) \cdot (\vec{u}_2 - \vec{u}_1)$. The vector sum of these components is the full force; the corresponding tensor-valued coefficient is $\widetilde{K} = C_\perp [\hat{n}\hat{n} + (C_\mu)(\widetilde{I} - \hat{n}\hat{n})]$ in which the ratio of coefficients $C_\mu = C_\parallel / C_\perp$ is like a coefficient of sliding friction. For $C_\mu = 0$ the immersed boundary condition is free-

slip; for $C_\mu \to 1$ and $C_\perp \to \infty$, the immersed boundary condition is no slip. Hence, by gauging the coefficients properly, any internal boundary condition of interest can be achieved.

In this study, this boundary is represented by the markers are thought of as platelets with finite surface area and thickness. We set the normal velocity at the actuator (marker) surface to zero. This condition applied to each marker allows estimates of the local normal force. Then, assuming locally one-dimensional flow, we use simple gas dynamic relationships to relate changes in velocity to changes in pressure across the actuator, ultimately providing the normal component of force. Tangential forces are estimated assuming fully developed turbulent flow. This boundary condition provides an estimate of the local shear stress. The local force density $\vec{F}_D = \Delta PA/V\hat{e}_n + \tau A/V\,\hat{e}_t$ where ΔP is the pressure difference across the actuator, τ is the wall shear stress, A the total platelet area in the cell volume, V, with $\vec{e}_n$ and $\vec{e}_t$ the normal and tangential unit vectors, respectively. The momentum exchange coefficient $\tilde{K}$ can then be estimated at each time step using $\vec{F}_D$. Finally, by consideration of the combined internal energy plus fluctuational energy budget, a source to gas phase fluctuational energy (k_1) appears as a result of the force on the actuator. This is called the slip-production rate. On a unit volume basis, it is $(\vec{u}_2 - \vec{u}_1)\cdot(\theta_1\theta_2)\tilde{K}\cdot(\vec{u}_2 - \vec{u}_1)$ [17].

Using this model, we set out to study the effect of the time-dependent actuator force on the dynamical response of the jet turbulence. The following discussion presents the results of our initial comparisons of simulation with experiment.

3. INITIAL MODEL COMPARISONS WITH PIV DATA

The actuators (Figure 1) are constructed by placing markers in rectangular shapes distributed about the nozzle exit. It is important to note that the markers are *placed* on the computational grid, i.e., the grid does not depend on the marker locations, and vise versa. Each actuator, represented by a set of markers, undergoes a programmed rigid body oscillation about an axis normal to the nozzle radius. The oscillation frequency, phase, and tip-to-tip displacement are prescribed. Our model implicitly assumes that the actuator motion and shape, and therefore the marker motion and spatial relationships, are not affected by the gas phase. Figure 2 illustrates the construction of an actuator–nozzle system. The computational domain shown in Figure 3 is a 19-block, pie-shaped sector that brackets a 3-actuator subset of the 13-actuator assembly. A cut-away view of the computational grid shows the 3 embedded actuators. The lateral boundaries (i.e., surfaces between the outboard actuators) are planes of symmetry and the upstream and downstream faces of the computational volume are assumed to be at constant pressure with inflow permitted. Constant inflow conditions $[\rho_1, \vec{u}_1, T_1]$ are specified at the nozzle entrance plane (~12.5 cm upstream of the nozzle exit). The actuators are oriented at an immersion angle of 24° with respect to the flow axis.

PIV data were taken at cross plane locations ranging from X/D = 0.125 to X/D = 6.0 as shown in Figure 4. Overall views of the flow field were constructed by first interpolating these data to a rectangular volume and then extracting interpolated data in various planes of interest. Profiles of normalized velocity (U/U_0) and turbulent kinetic energy (K/U_0^2) taken at X/D = 0.125, 0.75, 1.5, and 3.0 will be used in the following discussion. The reference velocity, U_0, is defined here as the ideal velocity resulting from an isentropic expansion of the plenum gas to ambient conditions. The nominal nozzle pressure ratio was 1.92 with stagnation temperature of 285 K, yielding $U_0 = 3.122 \times 10^4$ cm/sec.

Our approach is first to compare the measured and predicted flows without actuators, matching the model's initial and boundary conditions to the PIV data.[12] We then attempt to "tune" the momentum exchange coefficient $\tilde{K}$ by choosing effective values for the platelet thickness (d) to approximate the PIV data taken with *stationary* actuators. Finally, we use these boundary conditions and parameters to predict the changes in velocity and κ fields due to the moving actuators.

A. Baseline Flow Estimates

Figure 5 presents a comparison of the PIV data and simulation results for the nozzle without actuators and $0.125 \le$ X/D≤ 3.0. The dashed line in each plot locates the nozzle lip. In the near field, X/D≤ 0.5, the influence of the nozzle base region and the convergent nozzle can be seen in both the PIV and simulation

plots. Near the nozzle exit, the predicted values significantly under predict the shear layer growth rate and over predict the centerline velocity. For X/D ≥ 1.5, the influence of the base region and nozzle convergence diminishes and the comparison generally improves. The corresponding plots of K/U_0^2 in Figure 6 reflect these differences. Both the PIV and simulation predict a near-field peak in K/U_0^2 due to the base region of the nozzle. The simulation, however, shows a much sharper profile with a substantially larger peak value.

An examination of the computational grid reveals some possible explanations for these differences. The gridded base region height was constructed to be 0.051 cm while the actual fabricated height was 0.159 cm. This error leads to the calculation of higher gradients and larger than anticipated dissipation rates in the nozzle base region. Furthermore, the cell aspect ratio immediately adjacent to the nozzle base is greater than 10 and most likely lowers the model's numerical accuracy. Although its effect has not yet been analytically verified, the treatment of the base region affects our ability to directly compare experiment and simulation. In the discussion that follows, the influence of the base region grid should be kept in mind.

B. Stationary Actuator Performance Estimates

This is the first step in "tuning" the momentum exchange model. Figure 7 provides the comparison of velocity profiles downstream of a set of stationary actuators (e.g., F = 0 Hz). X/D is measured from the tip of the actuators for both PIV data and predictions. Profiles are extracted along the Z/D-axis in the Y/D=0 plane at various X/D locations. This means that the profiles are centered on the center actuator shown in Figure 3. (Across the nozzle, this profile would see a valley between actuators.) Since $\vec{F}_D$ varies as the inverse of the platelet thickness, smaller values of d produce greater momentum exchange (i.e., greater actuator authority). Note that in addition to generating drag, the actuators decrease the effective nozzle exit area, locally accelerating the flow.

The PIV data and simulation results are shown with the parameter d varying from 0.01 to 1.5. Although the trends are similar, the PIV data indicates a more rapid shear layer growth than the predictions at all axial stations. At X/D = 0.125, a d-value of 0.01 comes close to matching the core velocity, but the layer growth rate is much lower. Further downstream, the model consistently over predicts the centerline velocity by ~ 10-20%. Taken by itself, the trend with decreasing d makes sense: shear layer growth rates increase and centerline velocities decrease. Smaller values of d are currently being investigated.

The K/U_0^2 plots of Figure 8 compare the corresponding PIV and simulation profiles. The influence of the different base region treatment is again evident and produces trends similar to those observed in the baseline flow. The base region setup appears to dominate the predicted results with K/U_0^2 peak values about two times the PIV data at X/D = 0.125. At larger values of X/D, smaller values of d produce higher shear layer growth rates and lower peak values, showing the same trend as the measurements.

C. Active Actuator Performance Estimates

Figure 9 presents the programmed displacement and velocity of the actuators used for this comparison. The relative deflection (blue line) is the tip deflection from the static immersion angle (24°) divided by the maximum tip-to-tip displacement. The red line shows that tip velocities (red lines) reach 50 cm/sec, corresponding to maximum accelerations on the order of 10^5 cm/sec. Measured and predicted actuator performance data are presented in Figures 10 and 11. A platelet thickness of 0.01 cm taken from the stationary calculations above is used in the performance predictions. Each figure shows PIV and simulation data for stationary (F= 0 Hz) and time-averaged active (F=1450 Hz) cases. PIV and simulation data are shown by the solid and dashed lines, respectively. The PIV velocity data of Figure 10 show that actuation produces a slight increase in mixing rate and a reduction in core velocity for X/D = 0.125. Downstream, however, the 1450 Hz PIV data indicate that shear layer growth rates decrease slightly, indicating a relaxation of the initial growth rates. Although the base region effects discussed earlier cloud the model results, the trend is to increase mixing in the near-field and then relax to self-similar growth rates. Centerline velocities show little difference between the stationary and active cases for either set of data, indicating that the core flow is largely unaffected. Figure 11 shows the corresponding variation of K/U_0^2. The PIV data clearly show a substantial increase in the initial turbulence production rate that

quickly relaxes with downstream distance. The model mimics this trend, showing the broadening of the K/U_0^2 distribution and reduction of its peak with increasing X/D.

Finally, from this starting point, we focus on predicted performance results to demonstrate the potential usefulness of this approach. The stationary (F =0 Hz) case will be used as a basis for comparison. Instantaneous marker positions and corresponding normalized pressure contours in the Y/D = 0 plane are shown in Figure 12.a and 12.b. Red, blue, and black contour lines show the instantaneous pressure field at maximum, minimum, and stationary deflection angles. The corresponding marker positions are designated by the same color scheme. Note that the presence of the actuators alters the upstream flow field. The effect of the actuator motion is shown by the differences in location of a given pressure level. The lines of constant pressure resulting from the actuator motion occur everywhere *downstream* compared to those of the stationary case. Relative to the actuator surface, the pressure levels at maximum deflection (δ_{max}) and minimum deflection (δ_{min}) appear to shift with the actuator. Levels associated with δ_{max} lead on the upstream side (actuator moving up); the pressure levels at δ_{min} lead on the downstream side (actuator moving down). This is made clear in expanded view of Figure 12.b where the last three markers at each position are shown.

Figure 13 shows instantaneous contour maps of the *differences* between active and stationary pressure fields for
δ_{max} and δ_{min}. The pressure distribution changes dramatically between the two end conditions. At δ_{max} the downstream pressure is reduced compared to the stationary case. At δ_{min} the amount of pressure reduction decreases and regions of higher pressure occur in the core flow. Figure 14 illustrates the corresponding velocity fields. At δ_{max}, regions of low pressure correspond to increased velocity. High and low velocity regions corresponding to the actuator oscillations are evident on the centerline. By the time δ_{min} is reached, these disturbances are diminished in extent. Finally, Figure 15 presents the corresponding changes in turbulent kinetic energy. At δ_{max} relatively rapid changes occur across the initial shear layer and an alternating pattern of plus and minus changes exists downstream. At δ_{min}, the magnitude and extent of these changes has diminished.

4. SUMMARY

We have applied a general multifluid model developed by Los Alamos National Laboratory to describe the state of a cold jet perturbed by tab-type piezoelectric actuators. Initial comparisons of model predictions of axial velocity and turbulent kinetic energy with recent particle imaging velocimetry measurements have shown promise. The general nature of the predicted changes in velocity and turbulent kinetic energy production due to excitation were similar in to the experimental trends. The model supports the experimental observation that the actuators produce small changes in mixing rates near the nozzle exit plane that subsequently relax. (Far-field acoustic measurements at these conditions show a reduction in noise level and change in spectrum.) Shortcomings of the simulation grid, particularly in the nozzle base region, unfortunately diminished the fidelity of this comparison. Nonetheless, the feasibility and utility of the approach has been successfully demonstrated. Predicted variations of the principal flow parameters appear to be self-consistent with the actuator operation. We anticipate that improved gridding of the nozzle base region along with the model calibration approach outlined here will prove successful.

5. REFERENCES

1. Jubelin, B., 1980, "New Experimental Studies on Jet Noise Amplification," AIAA 80-0961
2. Crighton, D.G., 1981, "Acoustics as a branch of fluid mechanics," *J. Fluid Mech.*, **106**, pp. 261-98.
3. Hussain, A.K.M.F. and Zaman, K.B.M.Q., 1981, "The 'preferred mode' of the axisymmetric jet," *J. Fluid Mech*, **110**, pp. 39-71.
4. Ho, Chih-Ming and Huang, Lein-Saing, 1982, "Subharmonics and vortex merging in mixing layers," *J. Fluid Mech.*, **119**, pp. 443-473.
5. Gutmark, E. and Ho, C.M., 1983, "On the preferred modes and the spreading rates of jets," *Phys. Fluids,* **26** (10).
6. Ho, Chih-Ming and Huerre, Patrick, 1984, "Perturbed Free Shear Layers," Annual Reviews.
7. Wiltze, John M. and Glezer, Ari, 1993, "Manipulation of free shear flows using piezoelectric actuators," *J. Fluid Mech,* **249**, pp.261-285.

8. Parekh, D.E. et. Al., 1996, "Innovative Jet Flow Control: Mixing Enhancement Experiments," AIAA 96-0308.
9. Smith, B.L. and Glezer, Ari, 1997, "Vectoring and Small-Scale Motions Effected in Free Shear Flows Using Synthetic Jet Actuators," AIAA 97-0213.
10. Wiltze, John M and Glezer, Ari, 1998, "Direct excitation of small-scale motions in free shear flows," *Physics of Fluids*, **10**, Issue 8, pp. 2026-2036.
11. Davis, Staci A. and Glezer, Ari, 2000, "The Manipulation of Large- and Small-Scales in Coaxial Jets using Synthetic Jet Actuators," AIAA 2000-0403.
12. Butler, G. W. and Calkins, F. T, "Initial Attempts to Suppress Jet Noise Using Piezoelectric Actuators",
AIAA 2003-3193.
13. B. A. Kashiwa, and R. M. Rauenzahn, "A Multimaterial Formalism," Proceedings, ASME Symposium on Numerical Methods for Multiphase Flows, Lake Tahoe, NV, 19-23 June 1994.
14. B. A. Kashiwa, N. T. Padial, R. M. Rauenzahn, and W. B. VanderHeyden, "A Cell-Centered ICE Method of Multiphase Flow Simulations," Proceedings, ASME Symposium on Numerical Methods for Multiphase Flows, Lake Tahoe, NV, 19-23 June 1994.
15. M.W. Lewis, B. A. Kashiwa & R.M. Rauenzahn, "Hydrodynamic Ram Modeling with the Immersed Boundary Method", in Proceedings, ASME Pressure Vessels and Piping Conference, San Diego, CA, July 26-30, 1998.
16. C.S. Peskin 1977, "Numerical analysis fo blood flow in the heart", *J. Comput. Phys.*, **25**, 220-252.
17. B. A. Kashiwa and W.B. VanderHeyden, "Toward a General Theory for Multiphase Turbulence, Part I: Development and Guaging of the Model Equations", Los Alamos National Laboratory report LA-13773-MS (downloadable at http://public.lanl.gov/cfdlib-news/vtcpix/)

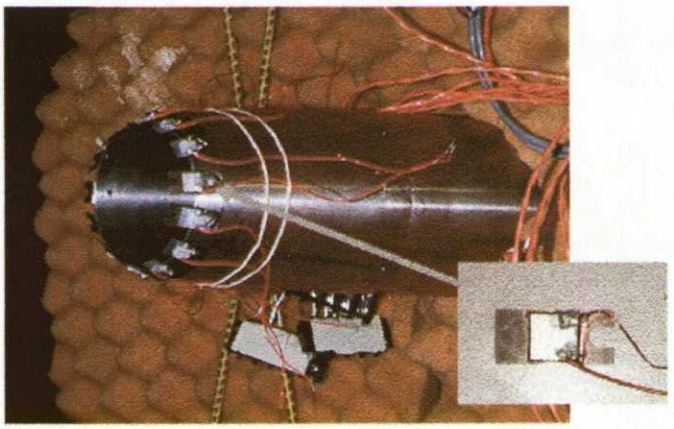

Figure 1. Integrated actuator-nozzle assembly mounted in Boeing's Quiet Air Facility. Nozzle diameter = 6.985 cm. There are 13 1.78 x 1.27 cm actuators. Insert shows an actuator.

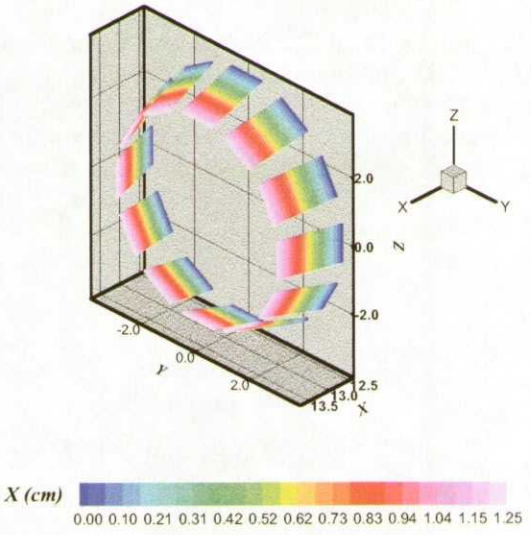

Figure 2. Construction of the actuator-assembly using marker particles. There are 992 markers/actuator and 13 actuators distributed at equal angles about the nozzle exit plane.

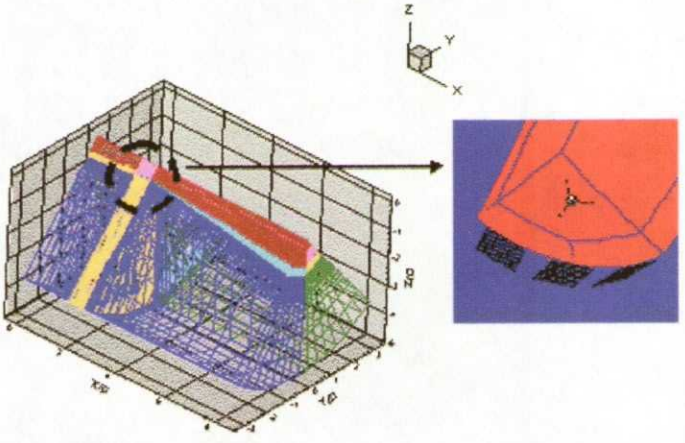

Figure 3. A 19-block finite volume grid encompassing a sector of the jet flow field. The expanded portion shows a cut away exposing three actuators positioned at the nozzle lip.

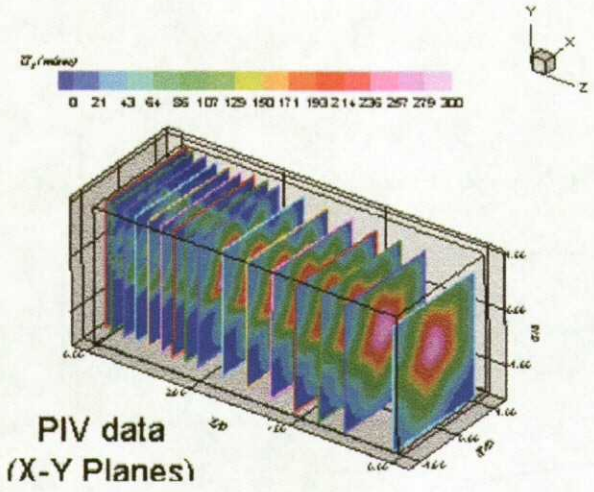

Figure 4. Example of particle imaging velocimetry data taken in planes normal to the jet axis. Profile data is extracted in the Y/D = 0 plane for comparison with predictions.

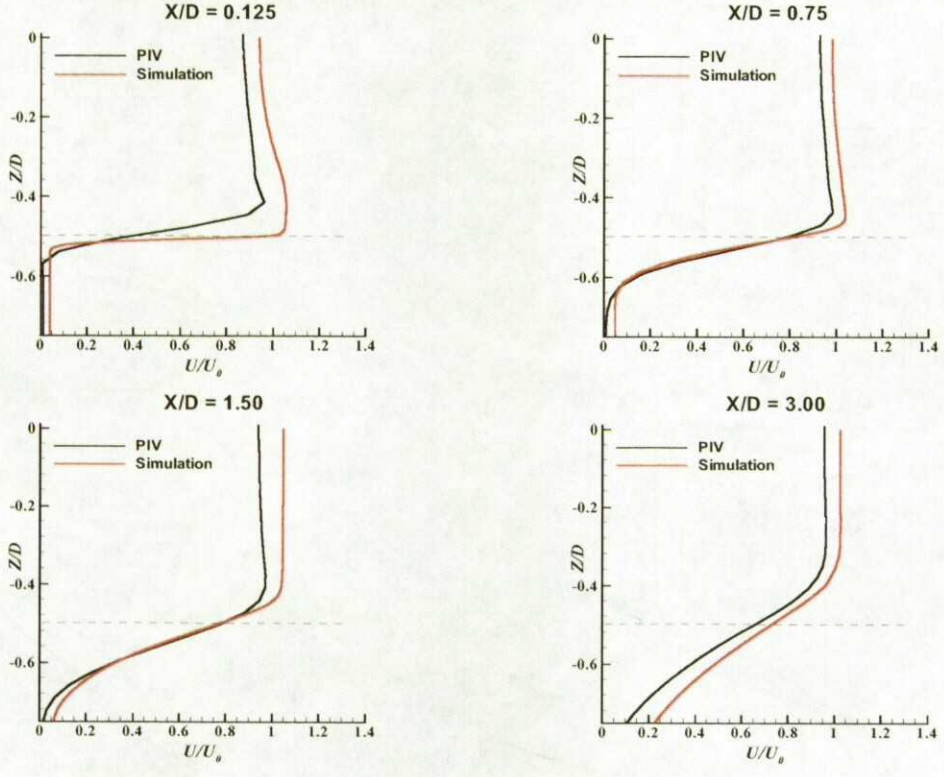

Figure 5. Plots of normalized velocity (U/U_0) for baseline nozzle taken along a vertical line at the nozzle exit. U_0=3.122x10^4 cm/sec. X/D = 0.125, 0.75, 1.5, and 3.00. Black lines are PIV data; red lines are model prediction

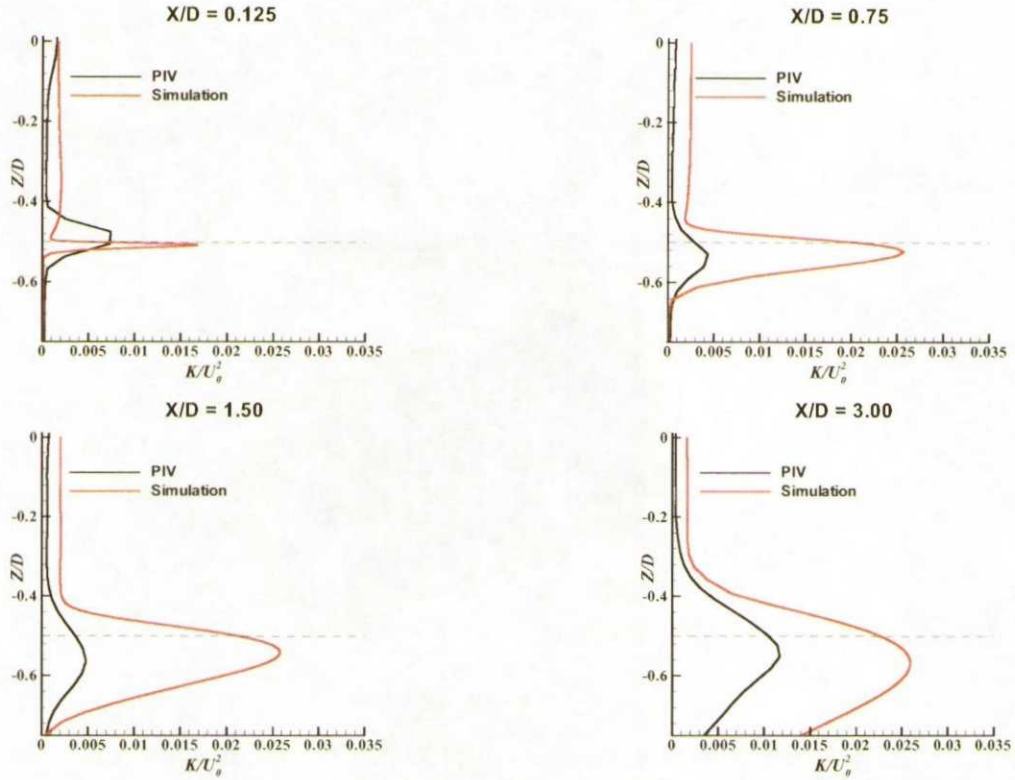

Figure 6. Plots of normalized turbulent kinetic energy (K/U_0^2)for the baseline nozzle taken along a vertical line from at the nozzle exit . U_0=3.122x10^4 cm/sec. X/D = 0.125, 0.75, 1.5, and 3.00. Black lines are PIV data; red lines are model predictions. The base region magnitudes strongly influence the prediction.

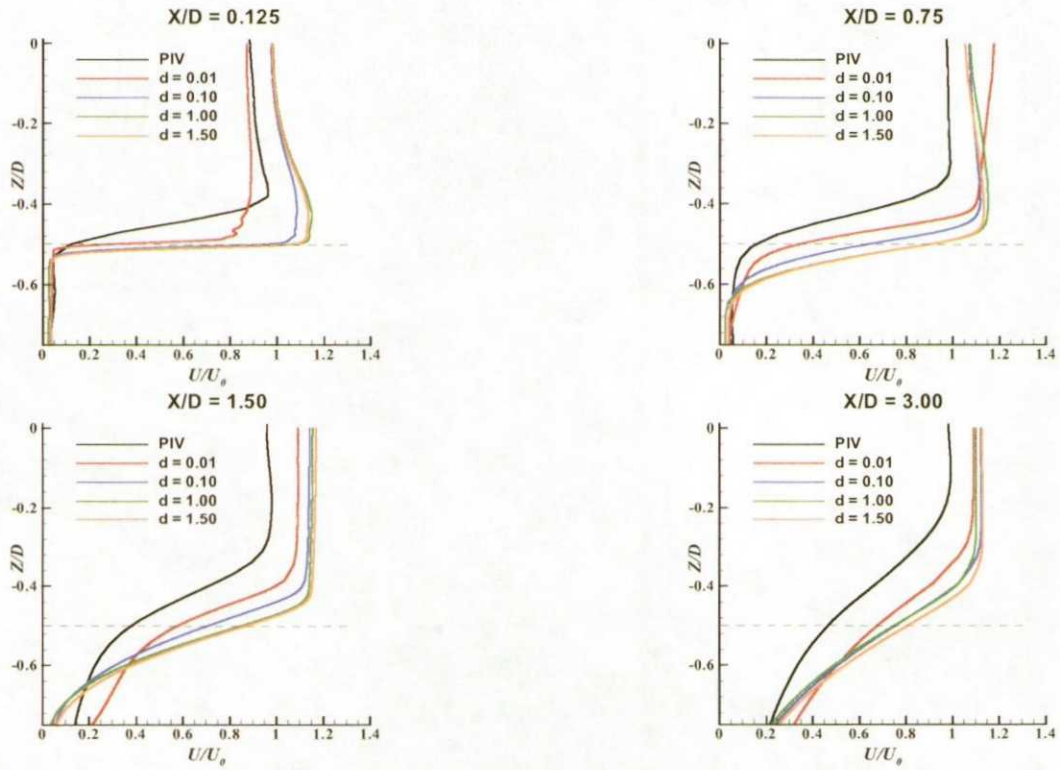

Figure 7. Plots of normalized velocity (U/U_0) for *stationary* actuators taken along a vertical line at the nozzle exit. U_0=3.122x10^4 cm/sec. Marker "thickness" d (cm) is the parameter.
X/D = 0.125, 0.75, 1.5, & 3.00.

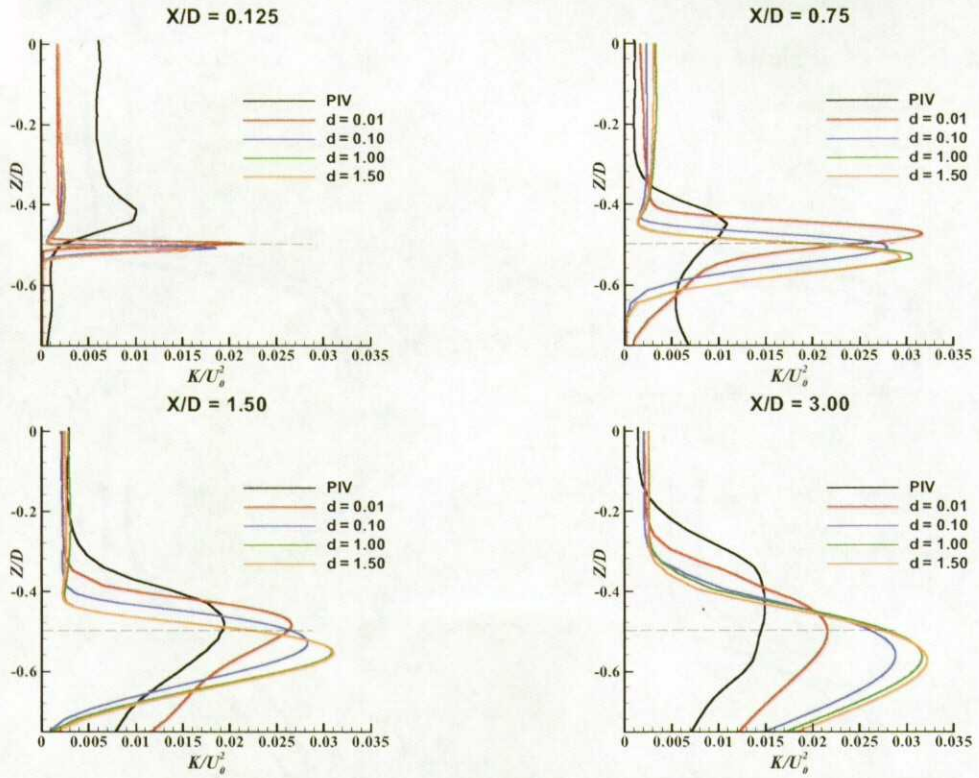

Figure 8. Plots of normalized turbulent kinetic energy (K/U_0^2) taken along a vertical line at the nozzle exit. U_0=3.122x10^4 cm/sec. Marker "thickness" d (cm) is the parameter. X/D = 0.125, 0.75, 1.5, & 3.00.

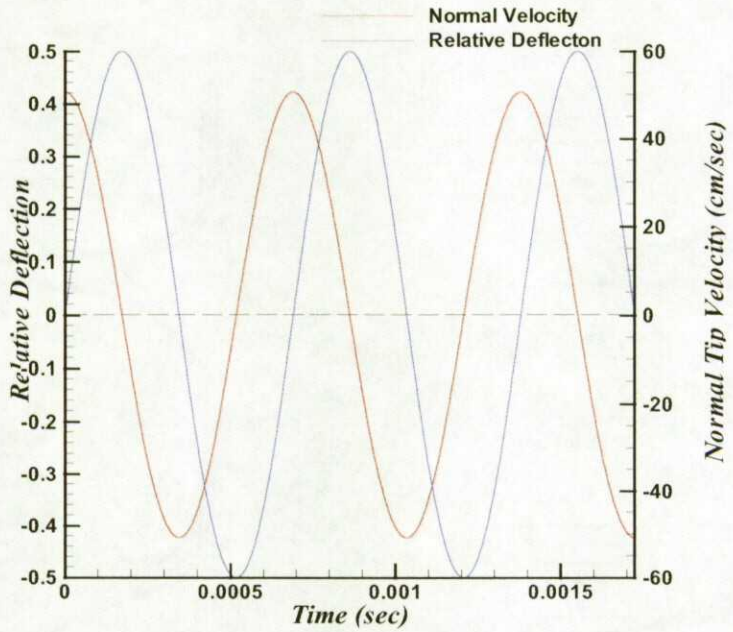

Figure 9. Programmed variation of actuator motion showing deflection relative to the immersed position and the tip velocity.

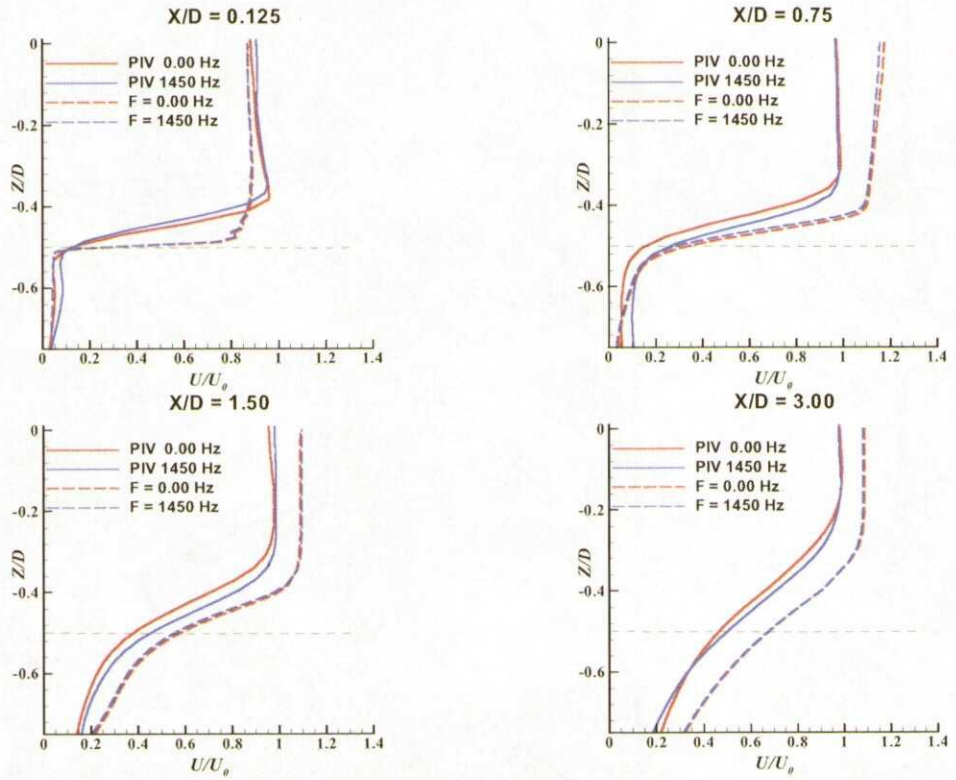

Figure 10. Plots of normalized velocity (U/U_0) for *active* actuators taken along a vertical line at the nozzle exit. F = 1450 Hz, U_0=3.122x10^4 cm/sec. X/D = 0.125, 0.75, 1.5, & 3.00.

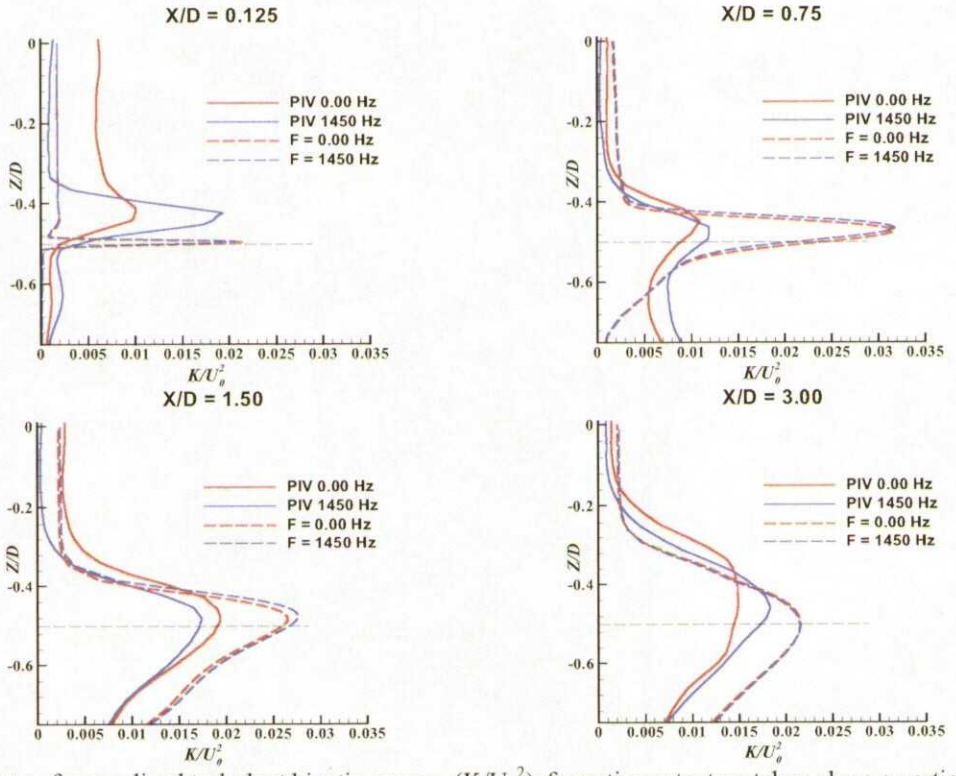

Figure 11. Plots of normalized turbulent kinetic energy (K/U_0^2) for active actuators taken along a vertical line at the nozzle exit. F = 1450 Hz, U_0=3.122x10^4 cm/sec. X/D = 0.125, 0.75, 1.5, & 3.00.

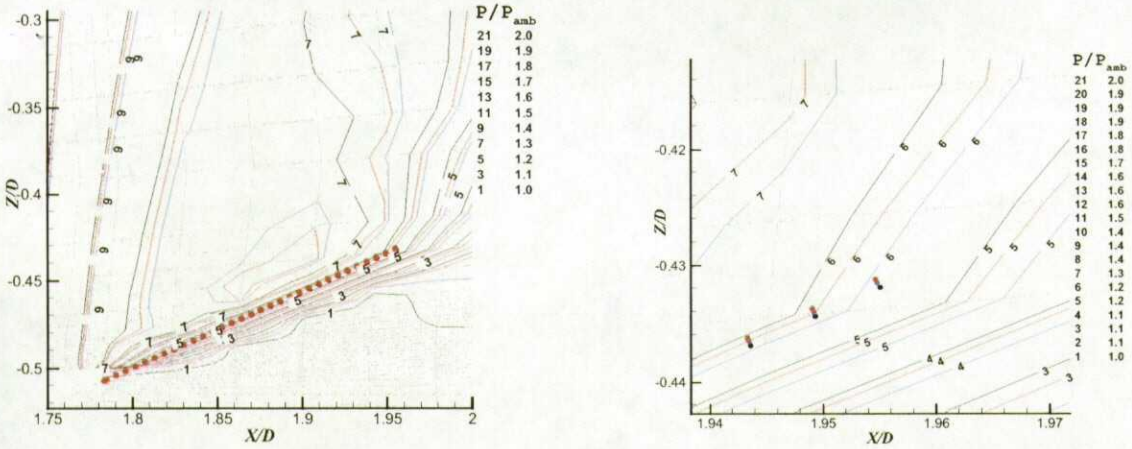

Figure 12. Instantaneous pressure fields produced by the actuator motion. Normalized by P_o = 1 atm. and referenced to a stationary actuator field. Red, blue, and black contour lines represent the maximum, minimum, and immersed positions. Markers representing the actuators are shown in corresponding colors. Grey background lines outline the computational grid.
a) Flow at the nozzle exit, b) Expanded view with the last three actuator markers for each position.

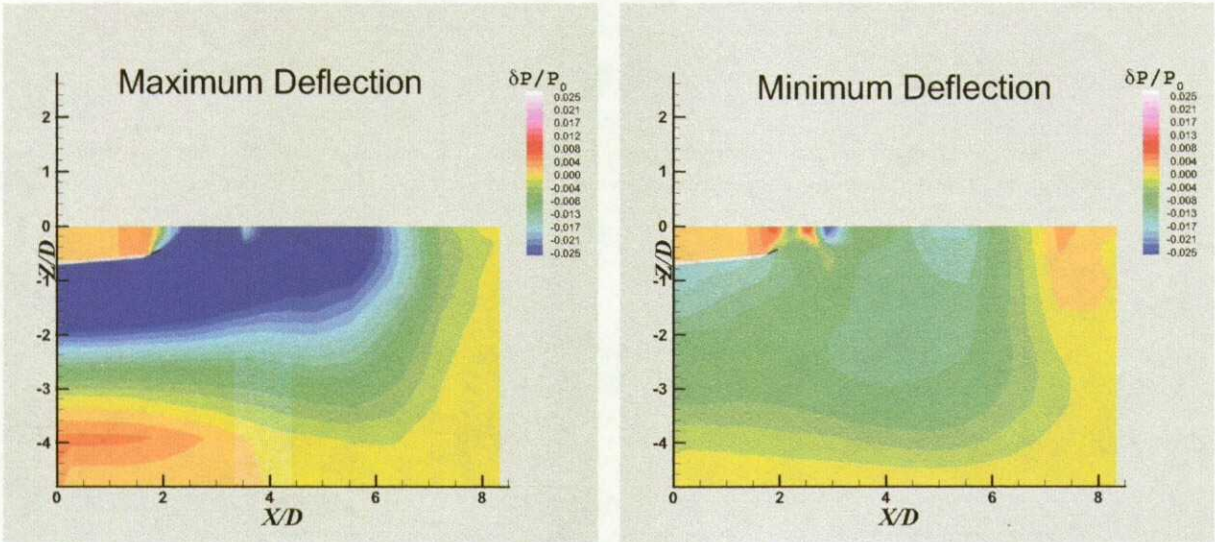

Figure 13. Instantaneous changes in pressure distribution at maximum and minimum actuator deflection. Referenced to the stationary actuator flow field and normalized by P_o = 1 atm.

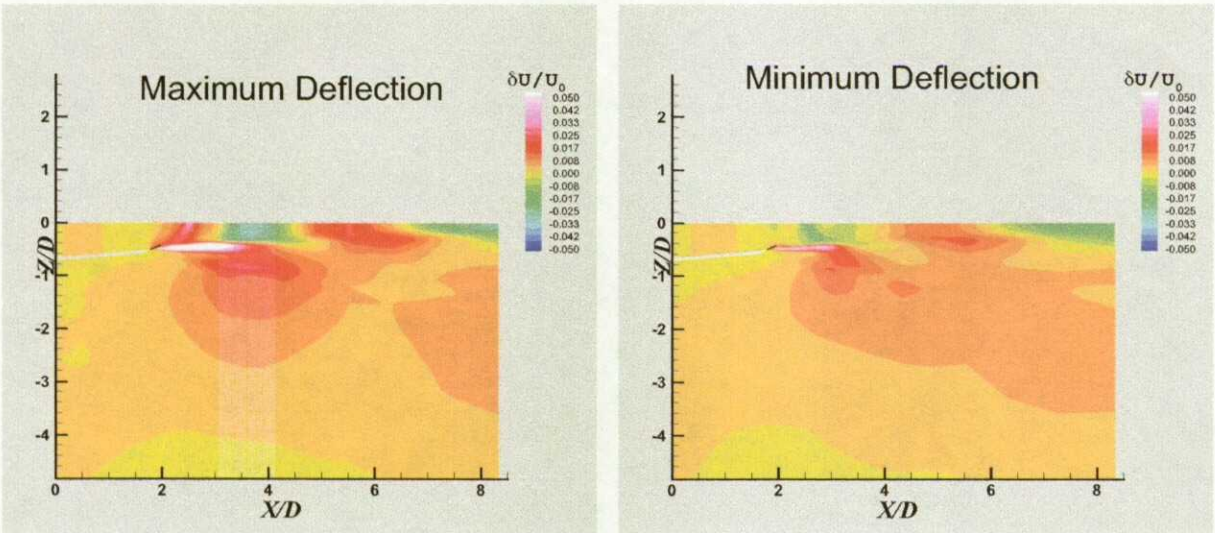

Figure 14. Instantaneous changes in velocity distribution at maximum and minimum actuator deflection. Referenced to the stationary actuator flow field and normalized by $U_o = 3.122 \times 10^4$ cm/sec.

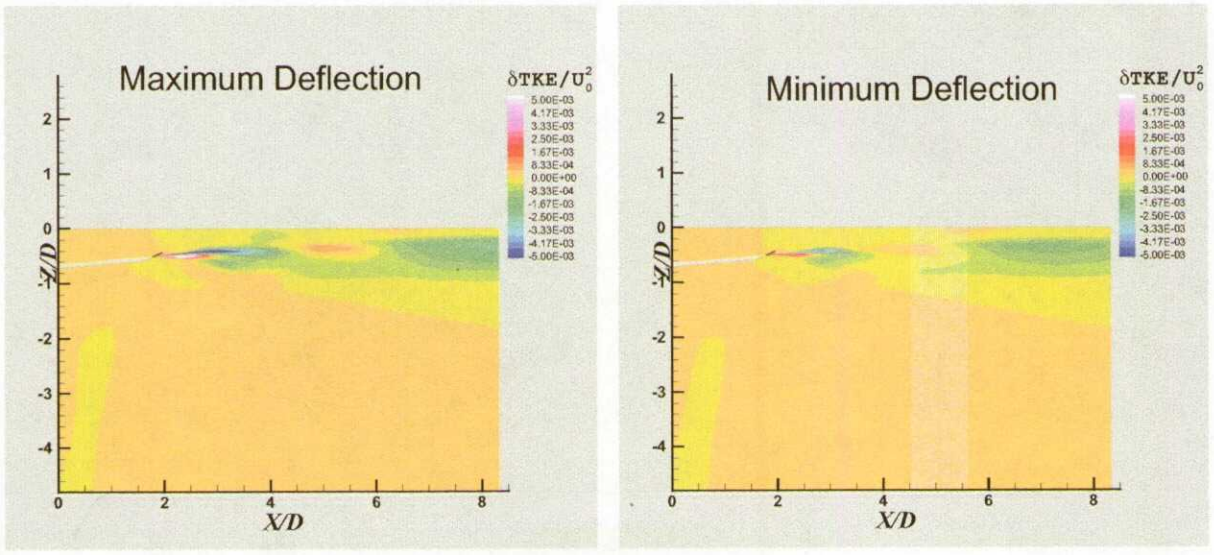

Figure 15. Instantaneous changes in turbulent kinetic energy distribution at maximum and minimum actuator deflection. Referenced to the stationary actuator flow field with $U_o = 3.122 \times 10^4$ cm/sec.